

# A New Framework for the Sum of Squared $\kappa$ - $\mu$ RVs with Application to Sub-THz Systems

Gustavo Rodrigues de Lima Tejerina and Italo Atzeni  
Centre for Wireless Communications, University of Oulu, Finland  
E-mail: {gustavo.tejerina, italo.atzeni}@oulu.fi

**Abstract**—In this paper, we adopt the  $\kappa$ - $\mu$  model to characterize the propagation in the sub-THz band. We develop a new exact representation of the sum of squared independent and identically distributed  $\kappa$ - $\mu$  random variables, which can be used to express the power of the received signal in multi-antenna systems. Unlike existing ones, the proposed analytical framework is remarkably tractable and computationally efficient, and thus can be conveniently employed to analyze systems with massive antenna arrays. We derive novel expressions for the probability density function and cumulative distribution function, analyze their convergence and truncation error, and discuss the computational complexity and the implementation aspects. Moreover, we derive expressions for the coverage probability and bit error probability for coherent binary modulations. Lastly, we evaluate the performance of an uplink sub-THz system where a single-antenna user is served by a base station employing maximum ratio combining.

**Index Terms**— $\kappa$ - $\mu$  distribution, sub-THz communications.

## I. INTRODUCTION

6G-and-beyond wireless systems are envisioned to explore the sub-THz spectrum, ranging from 100 to 300 GHz, to seek extreme bandwidths and accommodate an unprecedented number of users with high data rates [1]. In general, raising the carrier frequency has a two-fold impact on the propagation [2]. First, the penetration loss and roughness of the materials with respect to the wavelength increase: consequently, the impact of the non-line-of-sight (NLoS) paths tends to diminish and the line-of-sight (LoS) component becomes dominant. Second, the free-space path loss (for isotropic antennas) increases: thus, more antennas are needed to create physically large arrays that are capable of properly focusing the signal power.

Statistical channel characterization in the sub-6 GHz range typically employs the classical Rayleigh, Rice, and Nakagami- $m$  models. However, such models fail to properly capture the intricacies of the propagation at high frequencies, which motivates investigating more generalized ones such as the (Extended)  $\eta$ - $\mu$ ,  $\kappa$ - $\mu$ ,  $\alpha$ - $\mu$ ,  $\alpha$ - $\eta$ - $\kappa$ - $\mu$ , and fluctuating two-ray (FTR) models. For instance, [3]–[5] compared both classical and generalized fading models to measured data at 26, 28, 39, and 143.1 GHz in LoS and NLoS scenarios, showing a better fit for the generalized models. Other works investigated generalized fading models applied to specific scenarios including, e.g., multiple antennas [6], reflective surfaces [7], dual-hop communications [8], and random atmospheric absorption [9].

In this paper, we adopt the  $\kappa$ - $\mu$  model [10] to characterize the propagation in the sub-THz band. Indeed, the  $\kappa$ - $\mu$  model provides remarkable flexibility to represent scenarios with a dominant LoS component, which well fit the propagation at sub-THz frequencies. Moreover, it encompasses classical models such as Nakagami- $m$ , Rice, and Rayleigh. In multi-antenna systems with maximum ratio transmission (MRT) at the transmitter or maximum ratio combining (MRC) at the receiver, the power of the received signal can be expressed as a sum of squared random variables (RVs). In this regard, [11] proposed expressions for the probability density function (PDF) and cumulative distribution function (CDF) of the sum of squared independent and identically distributed (i.i.d.)  $\kappa$ - $\mu$  RVs employing special functions such as the modified Bessel function and Marcum Q-function. Additionally, evaluating the corresponding performance metrics either involves Horn functions [12], which are not readily available in common mathematical packages (such as Mathematica and SciPy), or requires cumbersome numerical integration. Hence, existing analytical frameworks become unsuitable to handle massive numbers of antennas due to their inherent computational complexity.

To address this issue, we extend the framework in [13] and develop a new exact representation of the sum of squared i.i.d.  $\kappa$ - $\mu$  RVs. The resulting framework is remarkably tractable and computationally efficient, and thus can be conveniently employed to study sub-THz systems with massive antenna arrays.<sup>1</sup> We derive novel expressions for the PDF and CDF, analyze their convergence and truncation error, and discuss the computational complexity and implementations aspects. Then, we derive expressions for the coverage probability and bit error probability (BEP) for coherent binary modulations, along with their asymptotic expressions at high signal-to-noise ratio (SNR). Lastly, we evaluate the performance of an uplink sub-THz system under the  $\kappa$ - $\mu$  model, where a single-antenna user is served by a multi-antenna base station (BS) employing MRC, with perfect and imperfect channel state information (CSI). For example, we observe that a  $4\times$  increase in the number of antennas allows the carrier frequency to be increased by about 60% while maintaining the same BEP. Moreover, even in LoS-dominated scenarios, the NLoS components continue to have a noticeable impact on the system's performance.

This work was supported by the Research Council of Finland (336449 Profi6, 348396 HIGH-6G, and 369116 6G Flagship) and by the European Commission (101095759 Hexa-X-II).

<sup>1</sup>Further results for the  $\kappa$ - $\mu$  model, along with an entirely new analysis using the Extended  $\eta$ - $\mu$  model applied to FR3 systems, can be found in the longer version of this paper [14].

**Notation.**  $f_X(x)$ ,  $F_X(x)$ , and  $\mathcal{M}_X(s)$  denote the PDF, CDF, and moment-generating function (MGF), respectively, of RV  $X$ .  $\text{erfc}(\cdot)$  is the complementary error function [15, Eq. (06.27.07.0001.01)],  $\Gamma(\cdot)$  is the Gamma function [15, Eq. (06.05.02.0001.01)] and  $\Gamma(\cdot, \cdot)$  is the incomplete Gamma function [15, Eq. (06.06.02.0001.01)].  $I_\nu(\cdot)$  denotes the modified Bessel function of the first kind and  $\nu$ -th order [15, Eq. (03.02.02.0001.01)].  ${}_pF_q(a_1, \dots, a_p; b_1, \dots, b_q; z)$ , for  $|z| < 1$  if  $q = p - 1$  or  $\forall z \in \mathbb{R}$  if  $q \geq p$ , is the generalized hypergeometric function [15, Eq. (07.31.02.0001.01)]. Lastly,  $\sim$  means asymptotically equivalent.

## II. NEW FRAMEWORK FOR THE SUM OF SQUARED $\kappa$ - $\mu$ RVs

Considering an  $N$ -antenna BS serving a single-antenna user, the sum of squared RVs can be used to express the instantaneous SNR in the downlink when the BS transmits data using MRT or in the uplink when the BS receives data using MRC. In this paper, we focus on the latter as our motivating scenario and for our performance evaluation, although the proposed framework also applies to the other setting [14]. In this context, the received signal after combining is given by

$$y = \mathbf{v}^H(\sqrt{P_t}\mathbf{h}x + \mathbf{z}) \in \mathbb{C}, \quad (1)$$

where  $\mathbf{v} \in \mathbb{C}^N$  is the combining vector,  $P_t$  is the transmit power,  $\mathbf{h} = [h_1, \dots, h_N] \in \mathbb{C}^N$  is the channel vector,  $x \in \mathbb{C}$  is the transmitted data symbol (with  $\mathbb{E}[|x|^2] = P_t$ ), and  $\mathbf{z} \in \mathbb{C}^N$  is the noise term with i.i.d.  $\mathcal{CN}(0, \sigma^2)$  entries. With perfect CSI, the MRC combining vector is given by  $\mathbf{v} = \mathbf{h}$  and the corresponding SNR at the BS is

$$\text{SNR}_P = \frac{P_t |\mathbf{v}^H \mathbf{h}|^2}{\sigma^2 \|\mathbf{v}\|^2} = \frac{P_t}{\sigma^2} \sum_{n=1}^N |h_n|^2. \quad (2)$$

Alternatively, assuming a simplified model for imperfect CSI, the MRC combining vector is given by  $\mathbf{v} = \hat{\mathbf{h}}$ , where  $\hat{\mathbf{h}} = \sqrt{1 - \alpha^2} \mathbf{h} + \alpha \tilde{\mathbf{h}} \in \mathbb{C}^N$  denotes the estimated channel,  $\tilde{\mathbf{h}} \in \mathbb{C}^N$  is the channel estimation error (independent of  $\mathbf{h}$ ) with i.i.d.  $\mathcal{CN}(\mathbf{0}, \frac{1}{N} \|\mathbf{h}\|^2)$  entries, and  $\alpha \in [0, 1]$  is the estimation accuracy (with  $\alpha = 0$  representing perfect CSI). When  $N \gg 1$ , the corresponding SNR at the BS can be approximated as  $\text{SNR}_I \simeq (1 - \alpha^2) \text{SNR}_P$ , with  $\text{SNR}_P$  defined in (2).

Motivated by the above system model, we propose a new exact representation of the sum of squared i.i.d.  $\kappa$ - $\mu$  RVs. The proposed framework is based on the recursive solution provided in [13] and results in much simpler expressions for the PDF and CDF (i.e., given in terms of simple Gamma functions) compared with [11], [12]. Hence, the resulting performance metrics, such as the BEP, also inherit the framework's simplicity. Furthermore, we analyze the convergence, truncation error, and computational complexity of these new expressions. The proposed framework has proven to return fast and precise solutions even with very large numbers of antennas.

### A. PDF and CDF

The  $\kappa$ - $\mu$  model is a generalized fading model used to represent scenarios with a dominant LoS component [10]. In this model,  $\kappa > 0$  denotes the power ratio between the LoS and NLoS (i.e., scattered) components, whereas  $\mu > 0$  indicates

the number of multipath clusters. For the  $\kappa$ - $\mu$  distribution, the PDF of the squared envelope of the  $n$ -th RV, denoted by  $W_n = \frac{P_t}{\sigma^2} |h_n|^2$ , is defined as [10]

$$f_{W_n}(w_n) = \frac{(\kappa + 1)^{\frac{\mu+1}{2}} w_n^{\frac{\mu-1}{2}} I_{\mu-1}(2\sqrt{\kappa\mu K \frac{w_n}{\hat{w}_n}})}{\mu^{-1} \kappa^{\frac{\mu-1}{2}} \hat{w}_n^{\frac{\mu+1}{2}} \exp(\kappa\mu + \frac{K w_n}{\hat{w}_n})}, \quad (3)$$

with  $w_n > 0$ ,  $K = (1 + \kappa)\mu$ , and  $\hat{w}_n = \mathbb{E}[W_n]$ . For the new representation of the sum of  $N$  squared i.i.d.  $\kappa$ - $\mu$  RVs, we follow the standard MGF-based approach to obtain the PDF: first, we derive the MGF of the squared RV and then we express the sum as the product of  $N$  MGFs.

For the first step, we begin by obtaining the MGF of (3) after applying the Laplace transform, i.e.,  $\mathcal{M}_X(s) = \int_0^\infty f_X(x) \exp(-sx) dx$ , as

$$\mathcal{M}_{W_n}(s) = \frac{\mu(\kappa + 1)^{\frac{\mu+1}{2}}}{\kappa^{\frac{\mu-1}{2}} \exp(\kappa\mu) \hat{w}_n^{\frac{\mu+1}{2}}} \int_0^\infty \frac{w_n^{\frac{\mu-1}{2}}}{\exp(s w_n)} \times \frac{I_{\mu-1}(2\sqrt{\kappa\mu K \frac{w_n}{\hat{w}_n}})}{\exp(\frac{K w_n}{\hat{w}_n})} dw_n. \quad (4)$$

Following the same rationale of [13], we rewrite the exponential and modified Bessel functions according to their contour integral representations [15, Eq. (03.02.07.0009.01), (01.03.07.0001.01)], which yields

$$\mathcal{M}_{W_n}(s) = \frac{j^{-1-\mu} \mu(\kappa + 1)^{\frac{\mu+1}{2}}}{4\pi^2 \kappa^{\frac{\mu-1}{2}} \hat{w}_n^{\frac{\mu+1}{2}} \exp(\kappa\mu)} \int_0^\infty \oint_{\mathcal{L}_t} \oint_{\mathcal{L}_v} \frac{w_n^{\frac{\mu-1}{2}} \Gamma(t)}{(s w_n)^t} \times \frac{\Gamma(v + \frac{\mu-1}{2}) (-\frac{\kappa\mu K w_n}{\hat{w}_n})^{-v}}{\Gamma(\frac{\mu-2v+1}{2}) \exp(\frac{K w_n}{\hat{w}_n})} dv dt dw_n, \quad (5)$$

where  $\mathcal{L}_t$  and  $\mathcal{L}_v$  are the complex contours of  $t$  and  $v$ , respectively. The integral operators in (5) are then reordered to solve the first one in terms of  $w_n$ , resulting in

$$\mathcal{M}_{W_n}(s) = \frac{j^{-1-\mu} (\kappa\mu)^{\frac{1-\mu}{2}}}{4\pi^2 \exp(\kappa\mu)} \oint_{\mathcal{L}_t^*} \oint_{\mathcal{L}_v^*} \frac{\Gamma(t) \Gamma(\frac{\mu-1}{2} + v)}{\Gamma(\frac{\mu+1}{2} - v) (-\kappa\mu)^v} \times \Gamma\left(\frac{\mu}{2} - t - v + \frac{1}{2}\right) \left(\frac{K}{s \hat{w}_n}\right)^t dv dt, \quad (6)$$

where  $\mathcal{L}_t^*$  and  $\mathcal{L}_v^*$  are the new complex contours of  $t$  and  $v$ , respectively, after the integration over  $w_n$ . At this stage, (6) has new essential singularities located at  $t \in \{-m, (-2l + \mu + 2m + 1)/2\}$  and at  $v \in \{(-2l - \mu + 1)/2, (-2l + \mu + 2m + 1)/2\}$ . As in [13], by identifying the singularities, the new complex contours are defined to guarantee the convergence of (6) and circumvent duplicate poles. With this in mind, both contour integrals can be solved by applying the residue theorem [16, Eq. (16.3.6)] to (6) for the poles  $t \rightarrow 1/2(\mu + 2m - 2v + 1)$  and  $v \rightarrow 1/2(-2l - \mu + 1)$ , leading to

$$\mathcal{M}_{W_n}(s) = \left(\frac{K}{\exp(\kappa) s \hat{w}_n}\right)^\mu \sum_{m=0}^\infty \sum_{l=0}^\infty \frac{\Gamma(l + m + \mu)}{m! l! \Gamma(l + \mu)} \times \left(\frac{\kappa\mu K}{s \hat{w}_n}\right)^l \left(-\frac{K}{s \hat{w}_n}\right)^m. \quad (7)$$

Finally, (7) is rearranged in terms of Cauchy product as

$$\mathcal{M}_{W_n}(s) = \left( \frac{K}{\exp(\kappa)s\hat{w}_n} \right)^\mu \sum_{m=0}^{\infty} \left( \frac{1}{s\hat{w}_n} \right)^m \sum_{l=0}^m \left( -\frac{1}{\kappa\mu} \right)^l \times \frac{(\kappa\mu K)^m \Gamma(m+\mu)}{l!(m-l)!\Gamma(m-l+\mu)}. \quad (8)$$

For the second step, the MGF of the sum of  $N$  i.i.d. RVs  $W_n$ , denoted by  $W = \sum_{n=1}^N W_n = \text{SNR}_p$ , is obtained as the product of their respective MGFs, i.e.,  $\mathcal{M}_W(s) = \prod_{n=1}^N \mathcal{M}_{W_n}(s)$ . From (8) and [17, Eq. (0.314)], this product is given by

$$\mathcal{M}_W(s) = \left( \frac{(\kappa+1)\mu}{\exp(\kappa)} \right)^{N\mu} \sum_{m=0}^{\infty} \left( \frac{1}{s\hat{w}} \right)^{N\mu+m} k_m, \quad (9)$$

where we have replaced  $\hat{w}_n = \hat{w}$ ,  $\forall n$  due to the i.i.d. property and with

$$k_0 = 1, \quad (10a)$$

$$k_m = \frac{1}{m} \sum_{i=1}^m (i-m+N)\Gamma(i+\mu)k_{m-i} \times \sum_{l=0}^i \frac{(-\kappa\mu)^{-l} (\kappa(\kappa+1)\mu^2)^i}{l!(i-l)!\Gamma(-l+i+\mu)}, \quad m \geq 1. \quad (10b)$$

Finally, the inverse Laplace transform is applied to (9) by using [17, Eq. (17.13.3)] and the PDF is obtained as

$$f_W(w) = \left( \frac{(\kappa+1)\mu}{\exp(\kappa)} \right)^{N\mu} \sum_{m=0}^{\infty} \frac{w^{N\mu+m-1} k_m}{\hat{w}^{N\mu+m} \Gamma(N\mu+m)}, \quad (11)$$

with  $k_m$  defined in (10). The CDF readily follows from applying  $F_X(x) = \int_0^x f_X(x) dx$ , which yields

$$F_W(w) = \left( \frac{(\kappa+1)\mu}{\exp(\kappa)} \right)^{N\mu} \sum_{m=0}^{\infty} \frac{\left( \frac{w}{\hat{w}} \right)^{N\mu+m} k_m}{\Gamma(N\mu+m+1)}. \quad (12)$$

An alternative MGF representation can be obtained from (7) by simplifying its  $m$ -indexed summation and reducing it to a power function, resulting in

$$\mathcal{M}_W(s) = \sum_{m=0}^{\infty} \frac{\tilde{k}_m}{\exp(N\kappa\mu)} \left( \frac{K}{K+s\hat{w}} \right)^{N\mu+m}, \quad (13)$$

with (cf. (10))

$$\tilde{k}_0 = 1, \quad (14a)$$

$$\tilde{k}_m = \frac{1}{m} \sum_{i=1}^m \frac{(Ni+i-m)(\kappa\mu)^i \tilde{k}_{m-i}}{\Gamma(i+1)}, \quad m \geq 1. \quad (14b)$$

From (13), the PDF is obtained as (cf. (11))

$$f_W(w) = \frac{\exp(-\frac{Kw}{\hat{w}})}{\exp(N\kappa\mu)} \sum_{m=0}^{\infty} \frac{\left( \frac{Kw}{\hat{w}} \right)^{N\mu+m} \tilde{k}_m}{w\Gamma(N\mu+m)}, \quad (15)$$

whereas the CDF is given by (cf. (12))

$$F_W(w) = \sum_{m=0}^{\infty} \left( 1 - \frac{\Gamma(N\mu+m, \frac{Kw}{\hat{w}})}{\Gamma(N\mu+m)} \right) \frac{\tilde{k}_m}{\exp(N\kappa\mu)}. \quad (16)$$

In Section III, we will use the PDFs in (11) and (15) to derive two distinct expressions for the BEP: one with lower computational complexity but quite restrictive convergence conditions, and another with slightly higher computational complexity and no restrictions on the convergence.

## B. Convergence and Truncation Analysis

We now analyze the infinite summations in (11)–(12) in terms of absolute convergence, which occurs when the sum of the absolute values of the individual terms converges [17, Eq. (0.21)]. Hence, we obtain an upper bound on the summations in (11)–(12), as done in [13]. Based on this, we derive the truncation error associated with the PDF and CDF, which provides useful insights into the number of terms needed to numerically compute these functions with the desired accuracy.

For the summations in (11)–(12), we need ensure that

$$\mathcal{C} = \sum_{m=0}^{\infty} \frac{w^{N\mu+m-1+\zeta} |k_m|}{\hat{w}^{N\mu+m} \Gamma(N\mu+m+\zeta)} < \infty, \quad (17)$$

where  $\zeta = 0$  and  $\zeta = 1$  correspond to (11) and (12), respectively. To this end, we first upper bound  $|k_m|$  for  $m \geq 1$  as

$$|k_m| < \sum_{i=1}^m \sum_{l=0}^i \frac{(i-m+N)\Gamma(i+\mu)K^i |k_{m-i}|}{ml!(i-l)!\Gamma(i-l+\mu)(\kappa\mu)^{l-i}}. \quad (18)$$

As  $1/\Gamma(i-l+\mu) \leq 1/\Gamma(\mu)$  for  $l \in [1, i]$  and  $1/\Gamma(\mu) < 8/7$  for any choice of  $\mu$ , we can upper bound the  $l$ -indexed summation of (18) by a power function [17, Eq. (1.111)], obtaining

$$|k_m| < \frac{8}{7m} \sum_{i=1}^m \frac{(i-m+N)\Gamma(i+\mu) |c_{m-i}|}{\Gamma(i+1) \tilde{K}^{-i}}, \quad (19)$$

with  $\tilde{K} = K(\kappa\mu+1)$ . Considering the last term of the summation (corresponding to  $i = m$ ) and the fact that  $1/\Gamma(m+1) < 1/\Gamma(m)$ , we obtain the simpler upper bound

$$|k_m| < \frac{8N\Gamma(\mu+m)}{7\Gamma(m)\tilde{K}^{-m}}. \quad (20)$$

Now, we extend (20) to all  $m$  by substituting the right-hand side of (20) into (17) and performing the index change  $m = i+1$ . After some mathematical manipulations, we obtain

$$\mathcal{C} < \frac{w^{N\mu-1+\zeta}}{\hat{w}^{N\mu}\Gamma(N\mu+\zeta)} \left( 1 + \frac{8N\Gamma(\mu+1)\Gamma(N\mu+\zeta)w}{7\Gamma(N\mu+1+\zeta)\hat{w}} \times \tilde{K} {}_1F_1\left(\mu+1; N\mu+1+\zeta; \frac{\tilde{K}w}{\hat{w}}\right) \right). \quad (21)$$

Finally, the absolute convergence of (17) and, consequently, the convergence of (11)–(12), follows from observing that the Kummer confluent hypergeometric function  ${}_1F_1$  in (21) is finite for any choice of parameters in our framework.

Moreover, we derive an upper bound on the truncation error when applied to (11)–(12). We begin by defining the truncation error as the sum of the truncated terms, i.e.,

$$\mathcal{E}(\epsilon) = \left( \frac{K}{\exp(\kappa)} \right)^{N\mu} \sum_{m=\epsilon}^{\infty} \frac{\left( \frac{w}{\hat{w}} \right)^{N\mu+m} k_m}{w^{1-\zeta} \Gamma(N\mu+m+\zeta)}, \quad (22)$$

where  $\epsilon$  indicates the number of terms employed to evaluate (11)–(12). From (22), we follow similar steps as those leading to (21) and, after some mathematical manipulations, we obtain

$$\mathcal{E}(\epsilon) < \left( \frac{K}{\exp(\kappa)} \right)^{N\mu} \frac{8N\Gamma(\mu+\epsilon)w^{N\mu+\epsilon-1+\zeta}}{7\Gamma(\epsilon)\Gamma(N\mu+\epsilon+\zeta)\hat{w}^{N\mu+\epsilon}} \times \tilde{K} {}_2F_2\left(1, \mu+\epsilon; \epsilon, N\mu+\epsilon+\zeta; \frac{\tilde{K}w}{\hat{w}}\right). \quad (23)$$

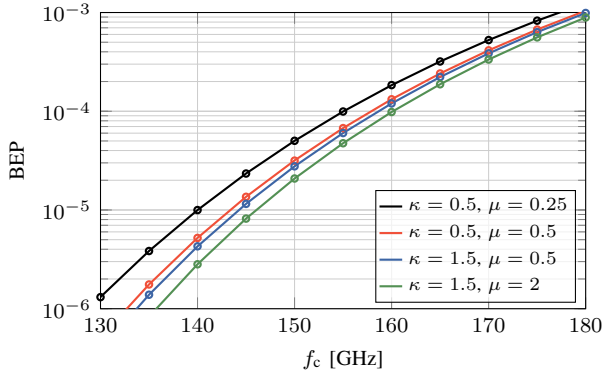


Fig. 1. PDF of the sum of squared i.i.d.  $\kappa$ - $\mu$  RVs, with  $N = 64$ ,  $\hat{w} = 1$ , and the following combinations of parameters: (i)  $\kappa \rightarrow 0$ ,  $\mu = 0.5$  (Nakagami- $m$ ); (ii)  $\kappa = 1.5$ ,  $\mu = 0.5$ ; (iii)  $\kappa = 1.5$ ,  $\mu = 1$  (Rice); and (iv)  $\kappa = 1.5$ ,  $\mu = 1.5$ .

### C. Computational Complexity and Implementation

As evinced by (10), the proposed framework uses recursion to numerically evaluate the derived expressions. A naive implementation would compute the same elements multiple times, which is highly inefficient when a large number of terms is involved. For example, by using the recursion tree method, the number of computations of the type of (10) amounts to  $2^\epsilon - 1$ . To reduce the computational complexity, we resort to memoization, a code optimization method that caches the value of every new recursive element, preventing the framework from computing it multiple times. With memoization, the number of computations of the type of (10) reduces to  $\epsilon(\epsilon + 1) - 1$ , enabling fast evaluation even with a large number of terms. Fig. 1 plots the analytical and simulated PDFs, with  $N = 64$ ,  $\hat{w} = 1$ , and different combinations of fading parameters. The analytical PDF is computed via (11) with truncation at  $\epsilon = 250$  terms, and strikingly agrees with the simulations. Remarkably, the computation time for each curve in the plots peaks at about 0.5 s and the maximum absolute error with respect to the exact solution in [11] is in the order of  $10^{-16}$ .

## III. PERFORMANCE METRICS

In this section, considering the system model and the results for the  $\kappa$ - $\mu$  distribution derived in Section II, we obtain new expressions for the coverage probability and BEP for coherent binary modulations. To evaluate the system's performance at high SNR, we further derive the asymptotic expressions for these metrics. In [14], we additionally analyze the symbol error probability for  $M$ -ary phase-shift keying and quadrature amplitude modulation.

### A. Coverage Probability

The coverage probability is defined as the probability that the instantaneous SNR exceeds a given threshold. This can be readily formulated in terms of the CDF of the instantaneous SNR, i.e.,  $P_{\text{cov}} = 1 - F_\gamma(\gamma_{\text{th}})$ , where  $\gamma_{\text{th}}$  is the SNR threshold. Hence, the coverage probability is readily available from (12), where  $\hat{w}$  is the scale parameter that can be used to model the path loss. To derive the asymptotic expression at high SNR,

as done in [18], we use only the first term of the summation (corresponding to  $m = 0$ ) in (12), resulting in

$$P_{\text{cov}} \sim 1 - \frac{1}{\Gamma(N\mu + 1)} \left( \frac{(\kappa + 1)\mu\gamma_{\text{th}}}{\exp(\kappa)\hat{w}} \right)^{N\mu}. \quad (24)$$

### B. BEP for Coherent Binary Modulations

We now focus on the (uncoded) BEP for coherent binary modulations. First, we obtain a new expression for the BEP by resorting to the PDF in (11), along with its asymptotic expressions at high SNR. Then, by deriving an upper bound on the BEP, we determine the convergence condition for this expression, which proves to be quite restrictive. To guarantee the convergence for any choice of parameters, we thus propose an alternative expression for the BEP based on the PDF in (15). Lastly, we obtain an upper bound on the truncation error.

The BEP for coherent binary modulations is defined as [19, Eq. (9.3)]

$$\text{BEP} = \frac{1}{2} \int_0^\infty \text{erfc}(\sqrt{g_b w}) f_W(w) dw, \quad (25)$$

with  $g_b = 1$  for coherent binary phase-shift keying (BPSK),  $g_b = 1/2$  for coherent orthogonal binary frequency-shift keying (BFSK), and  $g_b = 0.715$  for coherent BFSK with minimal correlation [19]. In our case,  $f_W(w)$  is replaced by the PDFs in (11) (or (15)).

**Approach 1.** By substituting (11) into (25), we obtain

$$\begin{aligned} \text{BEP} &= \frac{1}{2\sqrt{\pi}} \left( \frac{(\kappa + 1)\mu}{\exp(\kappa)} \right)^{N\mu} \sum_{m=0}^{\infty} \left( \frac{1}{g_b \hat{w}} \right)^{N\mu + m} \\ &\quad \times \frac{\Gamma(N\mu + m + \frac{1}{2}) k_m}{\Gamma(N\mu + m + 1)}. \end{aligned} \quad (26)$$

To derive the asymptotic expression at high SNR, we use only the first term of the summation (corresponding to  $m = 0$ ) in (26), resulting in<sup>2</sup>

$$\text{BEP} \sim \frac{\Gamma(N\mu + \frac{1}{2})}{2\sqrt{\pi}\Gamma(N\mu + 1)} \left( \frac{(\kappa + 1)\mu}{\exp(\kappa)g_b \hat{w}} \right)^{N\mu}. \quad (27)$$

Now, following similar steps as in Section II-B, we upper bound (26) as

$$\begin{aligned} \mathcal{C} &< \frac{1}{\hat{w}^{N\mu}} \left( \frac{\Gamma(N\mu + \frac{1}{2})}{\Gamma(N\mu + 1)} + \frac{8N\Gamma(\mu + 1)\Gamma(N\mu + \frac{3}{2})}{7\Gamma(N\mu + 2)} \right) \\ &\quad \times \frac{K}{g_b \hat{w}} {}_2F_1\left(\mu + 1; N\mu + \frac{3}{2}; N\mu + 2; \frac{K}{g_b \hat{w}}\right). \end{aligned} \quad (28)$$

Despite the strict convergence interval of the Gauss hypergeometric function  ${}_2F_1$ , common mathematical packages such as Mathematica and SciPy typically provide solutions with arguments outside the convergence interval through its analytical continuation. In our case, this feature could not be straightforwardly exploited for the summation in (26), restricting its convergence to choices of parameters satisfying  $|K/(g_b \hat{w})| < 1$ . To circumvent this issue and guarantee the convergence for any choice of parameters, we propose an alternative expression in the following.

<sup>2</sup>Note that (27) can also be obtained as a special case of the expression provided in [12].

$$\mathcal{E}(\epsilon) < {}_3F_2\left(N\mu + \epsilon + \frac{1}{2}, \mu + \epsilon, 1; N\mu + \epsilon + 1, \epsilon; \frac{K}{g_b\hat{w}}\right) \frac{4N\Gamma(\mu + \epsilon)\Gamma(N\mu + \epsilon + \frac{1}{2})}{7\sqrt{\pi}\Gamma(\epsilon)\Gamma(N\mu + \epsilon + 1)} \left(\frac{K}{g_b\hat{w}}\right)^\epsilon \left(\frac{(\kappa + 1)\mu}{\exp(\kappa)g_b\hat{w}}\right)^{N\mu} \quad (30)$$

**Approach 2.** By substituting (15) into (25), we obtain (cf. (26))

$$\text{BEP} = \sum_{m=0}^{\infty} \frac{\Gamma(N\mu + m + \frac{1}{2}) \left(\frac{\tilde{K}}{g_b\hat{w}}\right)^{N\mu + m} \tilde{k}_m}{2\sqrt{\pi} \exp(N\kappa\mu) \Gamma(N\mu + m + 1)} {}_2F_1\left(N\mu + m, N\mu + m + \frac{1}{2}; N\mu + m + 1; \frac{-\tilde{K}}{g_b\hat{w}}\right). \quad (29)$$

Remarkably, (29) allows to evaluate the BEP for any choice of parameters at the cost of slightly increased mathematical and computational complexity due to the presence of the Gauss hypergeometric function  ${}_2F_1$ . However, the computational complexity associated with this function can be drastically reduced by using its recurrence property [20, Eq. (15.5.E19)].

Lastly, by replicating the steps in Section II-B, we obtain an upper bound on the truncation error for the BEP in (30) at the top of the page, which applies to both approaches.

#### IV. PERFORMANCE EVALUATION

In this section, we build on the proposed framework for the  $\kappa$ - $\mu$  model to analyze the performance of an uplink system operating in the sub-THz band. As in the system model described in Section II, we consider a single-antenna user served by a multi-antenna BS employing MRC, with perfect and imperfect CSI. We compare the analytical results (obtained using Mathematica on a standard off-the-shelf laptop computer) with Monte Carlo simulations. In all the plots, the lines indicate the analytical results obtained with the proposed framework and the markers represent the simulation results, which are in agreement with the analytical results.

We assume a log-distance path loss model according to which we have  $\hat{w} = \frac{P_t}{\sigma^2} \varphi d^{-\beta}$ , where  $\varphi$  represents the frequency-dependent path loss factor referenced at 1 m,  $d$  denotes the distance between the user and the BS, and  $\beta = 2$  models the LoS-dominated propagation. The path loss factor is defined as  $\varphi = (c/(4\pi f_c))^2$ , where  $c$  represents the speed of light and  $f_c$  denotes the carrier frequency. The noise power is calculated as  $\sigma^2 = -174 + 10 \log_{10} \Omega + \nu$  (measured in dBm), where  $\Omega$  denotes the transmission bandwidth and  $\nu = 6$  dB is the noise figure of the BS. The bandwidth is set to 0.5% of the carrier frequency, i.e.,  $\Omega = 0.005 f_c$ . Unless otherwise stated, we fix  $P_t = 23$  dBm,  $f_c = 140$  GHz,  $d = 200$  m, and assume perfect CSI at the BS (i.e.,  $\alpha = 0$ ); furthermore we assume  $\kappa = 1.5$  and  $\mu = 0.5$  for the fading parameters.<sup>3</sup>

Fig. 2 plots the coverage probability versus the distance between the user and the BS, with  $\gamma_{\text{th}} \in \{0, 5\}$  dB. Adopting  $N = 512$  allows to compensate for the strong path loss at 140 GHz and achieve perfect coverage up to approximately

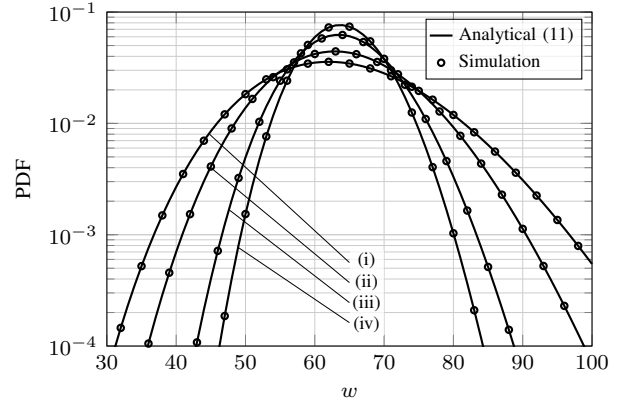


Fig. 2. Uplink coverage probability versus distance, with  $\kappa = 1.5$ ,  $\mu = 0.5$ ,  $f_c = 140$  GHz,  $P_t = 23$  dBm, and  $\alpha = 0$ .

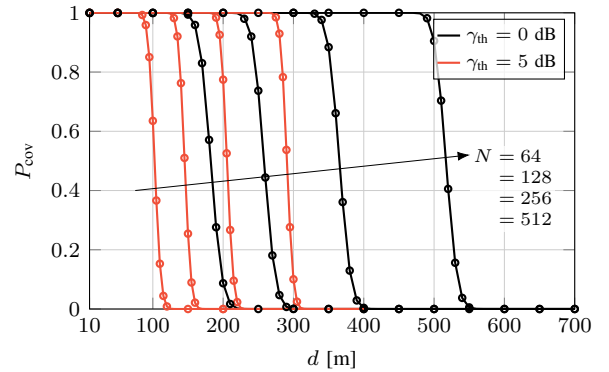


Fig. 3. Uplink BEP for coherent BPSK versus transmit power, with  $\kappa = 1.5$ ,  $\mu = 0.5$ ,  $f_c = 140$  GHz, and  $d = 200$  m.

250 m and 450 m for  $\gamma_{\text{th}} = 5$  dB and  $\gamma_{\text{th}} = 0$  dB, respectively. Note that this extensive coverage is primarily enabled by the truly massive number of antennas combined with the LoS-dominated propagation. The analytical results are computed with 500 terms, remarkably taking less than 5 s to generate the whole plot. For comparison, the expression in [11] provides the same output in about 105 s.

Fig. 3 illustrates the BEP for coherent BPSK versus the transmit power along with the asymptotic BEP at high SNR (dashed lines), with  $\alpha \in \{0, 0.4\}$ . Note that the asymptotic BEP is only depicted for  $N = 64$  to improve the readability of the plot. For  $P_t = 23$  dBm, doubling the number of antennas from  $N = 256$  to  $N = 512$  results in a  $36\times$  reduction in the BEP with  $\alpha = 0$ , i.e., from  $5 \times 10^{-3}$  to  $1.4 \times 10^{-4}$ . Furthermore, the asymptotic slopes are mainly dictated by the number of antennas and the number of multipath clusters. The analytical results are computed with no more than 500 terms and the entire plot is generated in less than 3 s.

Fig. 4 depicts the BEP for coherent BPSK versus the carrier frequency, again with  $\alpha \in \{0, 0.4\}$ . Fixing a target BEP of  $10^{-3}$ , increasing the number of antennas from  $N = 128$  to

<sup>3</sup>The fading parameters depend on the specific propagation conditions and fitting them to realistic scenarios is beyond the scope of this paper. Instead, our focus is to demonstrate the efficiency of the proposed framework and evaluate the system's performance across different choices of parameters.



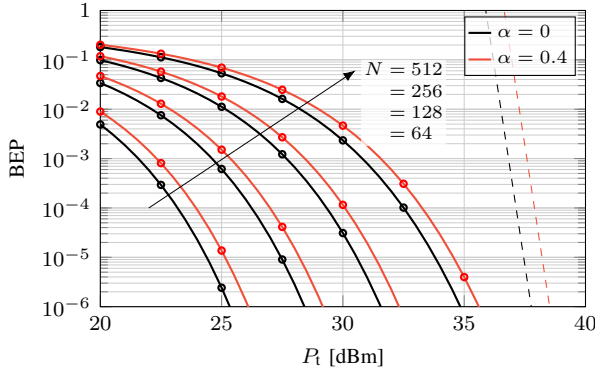


Fig. 4. Uplink BEP for coherent BPSK versus carrier frequency, with  $\kappa = 1.5$ ,  $\mu = 0.5$ ,  $d = 200$  m, and  $P_t = 23$  dBm.

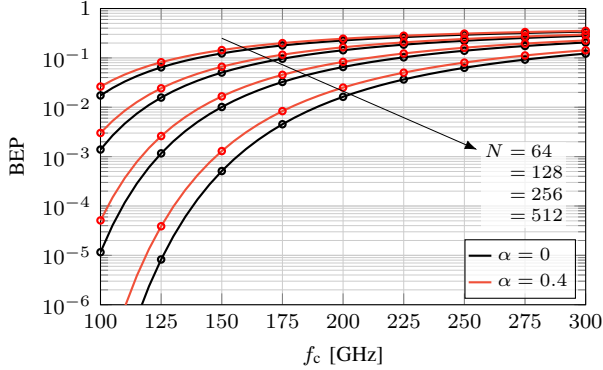


Fig. 5. Uplink BEP for coherent BPSK versus carrier frequency, with  $N = 128$ ,  $d = 80$  m,  $P_t = 23$  dBm, and  $\alpha = 0$ .

$N = 512$  allows the carrier frequency (and thus the bandwidth) to be increased by about 60%.

Fig. 5 shows the BEP for coherent BPSK versus the carrier frequency, with  $N = 128$ . We consider four combinations of fading parameters mimicking fading conditions ranging from very severe to favorable: (i)  $\kappa = 0.5$ ,  $\mu = 0.25$  (black line); (ii)  $\kappa = 0.5$ ,  $\mu = 0.5$  (red line); (iii)  $\kappa = 1.5$ ,  $\mu = 0.5$  (blue line); and (iv)  $\kappa = 1.5$ ,  $\mu = 2$  (green line). In (i), the BEP is undermined by the small value of  $\mu$  (i.e., the number of multipath clusters). In (ii), by slightly increasing  $\mu$ , the BEP significantly improves, which allows to push the carrier frequency up by at least 2 GHz. In (iii), a  $3\times$  increase in  $\kappa$  (i.e., the power ratio between the LoS and NLoS components) produces only a timid decrease in the BEP since the array gain weakly depends on  $\kappa$ . Lastly, in (vi), a bigger increase in  $\mu$  yields a considerable BEP improvement, further raising the carrier frequency by at least 1 GHz. Hence, even though we consider LoS-dominated propagation, the NLoS components still have a noticeable impact on the system's performance.

## V. CONCLUSIONS

In this paper, we developed a new exact representation of the sum of squared i.i.d.  $\kappa$ - $\mu$  RVs. The proposed analytical framework is remarkably tractable and computationally efficient, and thus can be conveniently employed to analyze system with massive antenna arrays. We derived novel expressions for the PDF and CDF, we analyzed their convergence and truncation

error, and we discussed the computational complexity and implementation aspects. Furthermore, we derived expressions for the coverage probability and BEP for coherent binary modulations. Lastly, we evaluated the performance of an uplink sub-THz system where a single-antenna user is served by a BS employing MRC. The results revealed that the number of antennas and the number of multipath clusters have the greatest impact on the system's performance. Future work will explore extensions to the multi-user scenario.

## REFERENCES

- [1] N. Rajatheva, I. Atzeni, E. Björnson *et al.*, "White paper on broadband connectivity in 6G," Jun. 2020. [Online]. Available: <https://oulurepo.oulu.fi/handle/10024/36799>
- [2] C. Han, Y. Wang, Y. Li, Y. Chen, N. A. Abbasi, T. Kürner, and A. F. Molisch, "Terahertz wireless channels: A holistic survey on measurement, modeling, and analysis," *IEEE Commun. Surveys and Tuts.*, vol. 24, no. 3, pp. 1670–1707, 2022.
- [3] T. R. R. Marins, A. A. D. Anjos, C. R. N. D. Silva, V. M. R. Peñarrocha, L. Rubio, J. Reig, R. A. A. De Souza, and M. D. Yacoub, "Fading evaluation in standardized 5G millimeter-wave band," *IEEE Access*, vol. 9, pp. 67 268–67 280, 2021.
- [4] E. N. Papasotiriou, A.-A. A. Boulogeorgos, K. Haneda, M. F. de Guzman, and A. Alexiou, "An experimentally validated fading model for THz wireless systems," *Sci. Rep.*, vol. 11, no. 1, p. 18717, 2021.
- [5] H. Du, J. Zhang, K. Guan, D. Niyato, H. Jiao, Z. Wang, and T. Kürner, "Performance and optimization of reconfigurable intelligent surface aided THz communications," *IEEE Trans. Commun.*, vol. 70, no. 5, pp. 3575–3593, 2022.
- [6] A. A. Joshi, P. Bhardwaj, and S. M. Zafaruddin, "Terahertz wireless transmissions with maximal ratio combining over fluctuating two-ray fading," in *Proc. IEEE Wireless Commun. and Netw. Conf. (WCNC)*, 2022.
- [7] N. P. Le and M.-S. Alouini, "Performance analysis of RIS-aided THz wireless systems over  $\alpha$ - $\mu$  fading: An approximate closed-form approach," *IEEE Internet of Things J.*, vol. 11, no. 1, pp. 1328–1343, 2024.
- [8] S. Li and L. Yang, "Performance analysis of dual-hop THz transmission systems over  $\alpha$ - $\mu$  fading channels with pointing errors," *IEEE Internet of Things J.*, vol. 9, no. 14, pp. 11 772–11 783, 2022.
- [9] P. Bhardwaj, R. Khanna, and S. M. Zafaruddin, "A generalized statistical model for THz wireless channel with random atmospheric absorption," in *Proc. IEEE Wireless Commun. and Netw. Conf. (WCNC)*, 2024.
- [10] M. D. Yacoub, "The  $\kappa$ - $\mu$  distribution and the  $\eta$ - $\mu$  distribution," *IEEE Trans. Antennas and Propag.*, vol. 49, no. 1, pp. 68–81, 2007.
- [11] M. Milisic, M. Hamza, and M. Hadzalic, "Outage performance of  $l$ -branch maximal-ratio combiner for generalized  $\kappa$ - $\mu$  fading," in *Proc. IEEE Veh. Technol. Conf. (VTC)*, 2008.
- [12] D. Dixit, P. Pandey, P. K. Verma, D. Sigroha, and D. K. Tripathi, "New exact ABER for MRC receiver in  $\kappa$ - $\mu$  faded channels," in *Proc. Int. Conf. IoT Commun. Autom. Technol. (ICICAT)*, 2023.
- [13] F. D. Almeida García, F. R. A. Parente, M. D. Yacoub, and J. C. S. S. Filho, "Exact  $\kappa$ - $\mu$  sum statistics," *IEEE Wireless Commun. Lett.*, vol. 12, no. 7, pp. 1284–1288, 2023.
- [14] G. R. d. L. Tejerina and I. Atzeni, "Sum of squared Extended  $\eta$ - $\mu$  and  $\kappa$ - $\mu$  RVs: A new framework applied to FR3 and sub-THz systems," *IEEE Trans. Wireless Commun.* (submitted), 2025. [Online]. Available: <https://arxiv.org/pdf/2502.02092>
- [15] (2001) The Mathematical Functions Site. Wolfram Research, Inc. Accessed: Oct. 19, 2023. [Online]. Available: <http://functions.wolfram.com/>
- [16] E. Kreyszig, *Advanced Engineering Mathematics*, 10th ed. Wiley Global Education, 2010.
- [17] I. S. Gradshteyn and I. M. Ryzhik, *Table of integrals, series, and products*, 7th ed. Elsevier/Academic Press, 2007.
- [18] F. D. Almeida García, F. R. A. Parente, M. D. Yacoub, and J. C. S. S. Filho, "On the exact sum PDF and CDF of  $\alpha$ - $\mu$  variates," *IEEE Trans. Wireless Commun.*, vol. 22, no. 8, pp. 5084–5095, 2023.
- [19] M. K. Simon and M.-S. Alouini, *Digital communication over fading channels*. John Wiley & Sons, 2005.
- [20] "NIST Digital Library of Mathematical Functions," Version 1.2.3; Release date 2024-12-15. [Online]. Available: <https://dlmf.nist.gov/>